Additive Manufacturing Letters 6 (2023) 100124

Contents lists available at ScienceDirect

Additive Manufacturing Letters

journal homepage: www.elsevier.com/locate/addlet

Short Communication

Non-equimolar Cantor high entropy alloy fabrication using metal powder cored wire arc additive manufacturing

Anatoliy Zavdoveev[a,*], Andrey Klapatyuk[a], Thierry Baudin[b], Eric MacDonald[c], Dhanesh Mohan[d], J.P. Oliveira[e], Alex Gajvoronskiy[a], Valeriy Poznyakov[a], Hyoung Seop Kim[f], Francois Brisset[b], Maksym Khokhlov[a], Mark Heaton[g], Massimo Rogante[h], Mykola Skoryk[i], Dmitry Vedel[j], Roman Kozin[a], Illya Klochkov[a], Sviatoslav Motrunich[a]

[a] *Paton Electric Welding Institute of NAS of Ukraine, K.Malevicha 11, Kiev 03150, Ukraine*
[b] *Université Paris-Saclay, CNRS, Institut de Chimie Moléculaire et des Matériaux d'Orsay, Orsay 91405, France*
[c] *University of Texas at El Paso, TX 79968, United States*
[d] *Department of Material Processing Engineering, Zhengzhou Research Institute of Harbin Institute of Technology, Zhengzhou, China*
[e] *CENIMAT/I3N, Department of Materials Science, NOVA School of Science and Technology, Universidade NOVA de Lisboa, Caparica 2829-516, Portugal*
[f] *Department of Materials Science and Engineering, (POSTECH), Pohang University of Science and Technology, Pohang 37673, South Korea*
[g] *ANT, Advanced Nano Technology, Park West Business Park, Nandor Rd, Dublin, Ireland*
[h] *Rogante Engineering Office, Contrada San Michele n.61, Civitanova Marche 62012, Italy*
[i] *G. V. Kurdyumov Institute of Metal Physics of the NAS of Ukraine, Kyiv, Ukraine*
[j] *I.M. Frantsevich Institute of Problems of Materials Science NAS of Ukraine, st. Krzyzanowski, Kyiv 303142, Ukraine*

ARTICLE INFO

Keywords:
High entropy alloy
Wire arc additive manufacturing
Metal powder cored wire
Mechanical properties
Structure

ABSTRACT

In the current contribution, the wire arc additive manufacturing of non-equimolar Co-Cr-Fe-Mn-Ni high-entropy alloy using gas metal arc welding (GMAW) with metal powder-cored wire (MPCW) is proposed. The powder's filler of designed wire feedstock contains Co-Cr-Mn-Ni components in equal atomic amounts relative to each other with Fe metal stripe as a shield. The proposed method provides the possibility to build bulk high-entropy alloy samples with the desired characteristics. The current work approach is superior in a number of indicators to such alternative methods of obtaining bulk HEAs as melting in vacuum, plasma arc melting, selective laser melting, or electron beam melting.

1. Introduction

High entropy alloys (HEAs) are defined as those composed of five or more principal elements with the elemental content typically ranging between 5 and 35 at. %. Several alloy systems have been developed with simple crystal structures and remarkable properties [1] and HEAs are becoming recognized for being composed of a variety of microstructures: single-phase FCC, BCC, or HCP [2–4], or even more complex multi-phase microstructures [5]. Consequently, these alloys have attracted significant research interest owing to their promising properties observed over wide temperature ranges and chemical environments. For instance, the quinary equimolar CrMnFeCoNi Cantor HEA possesses an exceptional fracture toughness of more than 200 MPa $m^{1/2}$ at cryogenic temperatures, rendering the alloy an ideal material for low-temperature applications. The standard methods to process HEAs include powder metallurgy [6], conventional casting [2,7], and additive manufacture (AM) [8–12]. Currently, there are a number of HEA utilized by various AM processes with different processing parameters, including CrMnFeCoNi [13,14], C-containing CrCoNiFe [15], YGdTbDyLu and $AlCo_xCr_{1-x}FeNi$ [3,16–19] HEAs.

The most recent widespread fusion-based AM methods can be classified as: electron-beam [8,11,12,19–21] and laser-based [22–24] powder bed fusion as well as wire arc additive manufacturing (WAAM) [25,26]. The advantages of the electron-beam and laser-based powder bed fusion include the smaller grain size of the fabricated parts which is explained

Abbreviations: AM, additive manufacturing; BCC, body-centred cubic; BSE, backscattered elecrtons; E, Young's modulus; EBSD, electron backscattered diffraction; EDX, energy dispersive X-Ray analysis; FCC, face-centred cubic; GB, grain boundary; GMAW, gas metal arc welding; H, Meyer hardness; HCP, hexagonal close package; HEA, high entropy alloy; HV, Vickers hardness; MPCW, metal powder-cored wire; SE, secondary electrons; SEM, scanning electron microscopy; SGB, sub grain boundary; UTS, ultimate tensile stress; WAAM, wire arc additive manufacturing; WTC, welding thermal cycle; YS, yield stress.

* Corresponding author.
E-mail addresses: avzavdoveev@gmail.com, zavdoveev@paton.kyiv.ua (A. Zavdoveev).

https://doi.org/10.1016/j.addlet.2023.100124
Received 29 November 2022; Received in revised form 25 January 2023; Accepted 25 January 2023

Table 1
Chemical composition of the metal stripe used for wire feedstock fabrication (in wt.%).

C	Si	Mn	Ni	S	P	Fe
0.05	0.05	0.35	≤0.30	≤ 0.04	≤ 0.035	balance

by the smaller heat source dimensions and associated faster cooling rate. A disadvantage of powder bed fusion in the case of HEAs is the problem of getting powders with high entropy alloy composition i.e. separate powder should already have the HEA composition for achieving homogeneous phase composition in the final product. One of the most promising directed energy deposition AM methods is WAAM [25,26], a cost-effective process in which melting of the feedstock material is induced by an electric arc. Commercially available welding wires can be used as feedstock for WAAM, circumventing the high costs and potential safety concerns associated with metal powders. Directed energy deposition, in which the WAAM process is subsumed, is attracting substantial industrial attention for large and complex structures. The powder wire is beneficial in comparison with solid wire [25] due to difficulties of the production of last. Either drawing of the solid wire or combining several thin wires in one cord [26]. The main disadvantages of these methods are the limitation of the production of wires of a certain chemical composition for the creation of cord wires, which allows obtaining the required chemical composition of the WAAM metal.

Thus, in the current work, it is proposed a new innovative approach for bulk HEAs fabrication using WAAM where, as a feedstock, the designed metal powder-cored wire is used. It is shown that the developed MPCW feedstock allows for obtaining HEA composition in the WAAM bulk sample. A successful attempt has been made for Fe-rich bulk non-equimolar CoCrFeMnNi high entropy alloy sample fabrication. The evaluation of microstructure and mechanical properties is performed highlighting the potential for WAAM to be used for the creation of large structural components composed of these promising HEAs. And finally it has been shown the way for cost-effective production of the bulk HEAs of complex alloying systems.

2. Experimental procedure

2.2. Metal powder cored wire (MPCW) manufacturing

For the production of the MPCW feedstock material used in this work, an ultra-low carbon steel (composition detailed in Table 1) stripe with a size of 0.4 × 10 mm was used with a filling coefficient set to 60%. The metals powders used for the MPCW wires had the following features: Ni - ball-shaped particles with a size of ≈ 100 μm and purity of 98% (refer to Fig. 1 a); Mn and Cr – sharped bricks-like particles having a size distribution of 100-300 μm and a purity of 94 and 98%, respectively (Fig. 1 a); Co – leaf-like morphology with an average size of 20 μm and purity of 98% (Fig. 1 a).

The steel strip was placed into forming rolls and eventually the raw powders were added onto the surface of the steel after which enveloping rolls were used to create the wire-shaped feedstock composed of an outer layer of the steel strip and within by raw powder including Ni, Mn, Cr and Co. After the enveloping stage, wire drawing until a final diameter of 2.4 mm was obtained. Here, it should be mentioned that multiple drawing steps were performed to avoid diameter reductions of over 23 % in a single draw [27]. Hence, the MPCW wire drawing route was performed as follows: diameter = 3.8 to 3.4, 3.0,2.75 and finally to 2.4 mm (with associated partial reductions of 20, 22, 16 and 23%, respectively). The average composition of the wire core filler powder mixture was determined to be 25% Cr, 25% Mn, 25% Co, and 25% Ni at.%. A schematic representation of the MPCW feedstock manufacturing route as well as a cross-section view is detailed in Fig. 1 b, c.

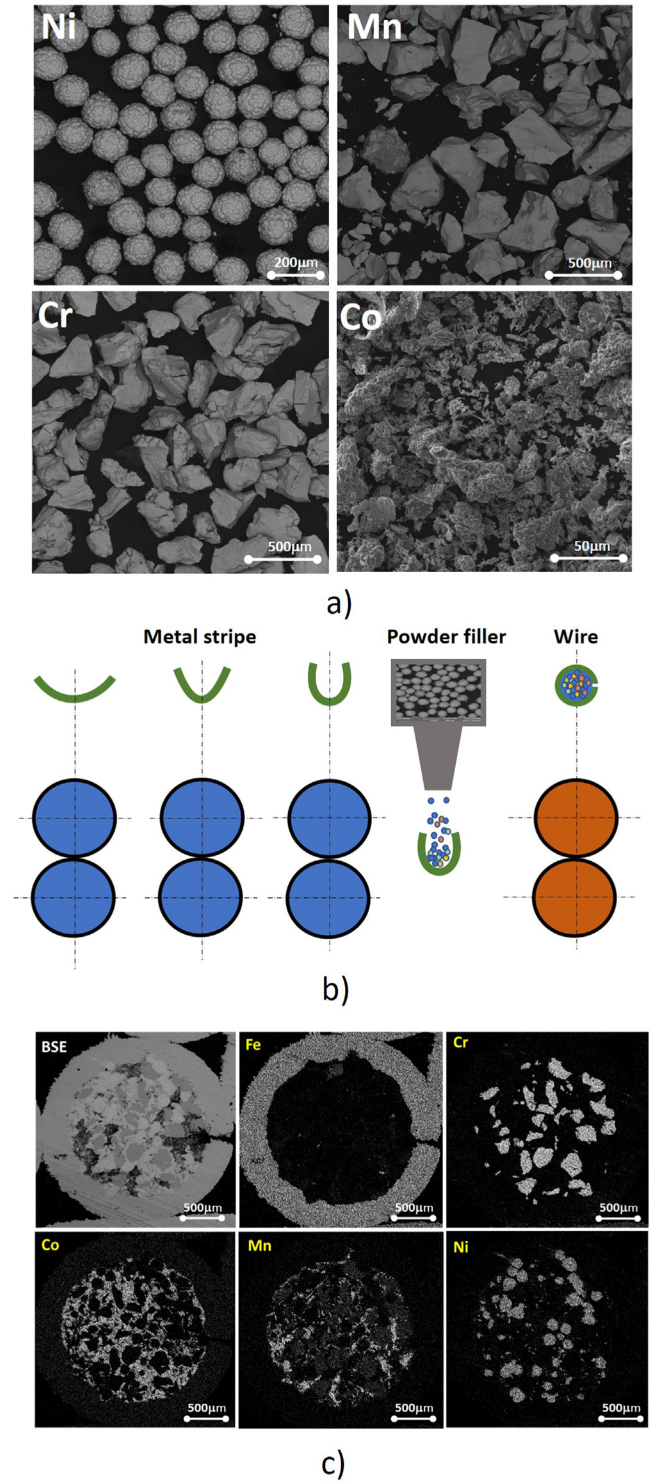

Fig. 1. The metal powder-cored wire manufacturing details: initial powders (a), manufacturing route (b), SEM and X-Ray maps of the manufactured MPCW cross-section (c).

The final MPCW was analysed by energy dispersive spectroscopy (EDS) over the cross section as detailed in Fig. 1 c. Although mixing of the raw powders is not homogenous, this is not expected to be an issues for WAAM since both the inner and outer regions of the wire are ultimately melted and then mixed within the melt pool.

Table 2
Deposition parameters used in this work.

Welding mode	Wire diameter (mm)	Current (A)	Voltage (V)	Welding speed (mm/s)	Tip to work distance (mm)	Gas flow (Ar+18%CO_2) (l/min)	Interpass temperature (°C)
GMAW	2.4	280-350	32-34	4	24	20-25	200-250

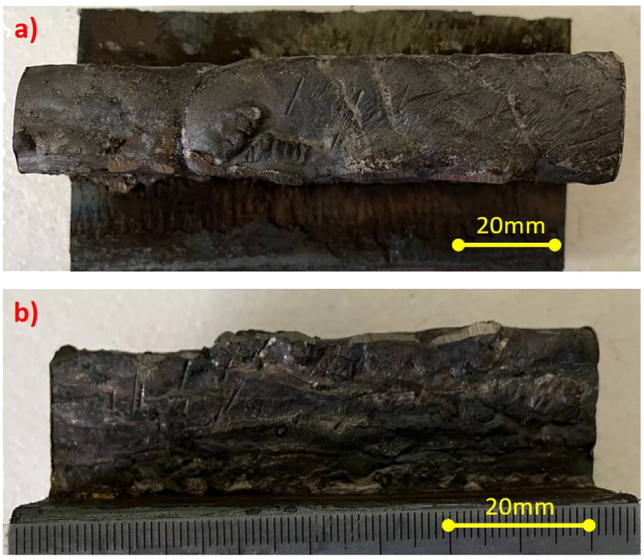

Fig. 2. Bulk WAAM fabricated non-equimolar CoCrFeMnNi HEA: (a) top view; (b) side view.

2.2. Manufacturing of non-equimolar CoCrFeMnNi by WAAM

A directed energy deposition tool encompassing a welding power supply VDU-506 was used for melting and depositing the MPCW feedstock material. The deposition parameters for metal deposition included a current ranging from 280 to 350 A and an arc voltage between 32 and 34 V. The depositions for each layer were performed when the previously deposited layer temperature was between 200 and 250°C. To achieve stable deposition conditions, the wire feed speed was varied between 77 and 90 mm/s. The full list of the deposition parameters is detailed in Table 2.

A WAAM wall with a total of ten layers was deposited. The monolithic sample measured 150 × 35 × 20 mm (Fig. 2). The deposition was made on the high strength low alloy steel substrate with a width of 50 mm and thickness of 14 mm. According to the Archimedes method, the density of the alloy was measured at 7.771±0.072 g/cm^3

As can be seen, WAAM using developed MPCW is beneficial from the analogous technique of additive manufacturing and conventional casting process. From the point of view of WAAM with solid wire or cord wire, MPCW increases the compositional working window allowing wider governing of the alloying. Concerning conventional casting, the designed technology based on MPCW during WAAM, gives the opportunity to fabricate bulk billets at lower cost and time limits.

2.3. Material characterization

The preparation of metallographic specimens for microstructural studies was implemented according to standard methods using grinding papers of various roughness. Final polishing was performed on a diamond suspension with an average polishing particle size of 1 μm. To reveal and identify the morphology of the macrostructure of the WAAM parts, etching with a 15 ml HCl_3 + 5 ml HNO_3 solution was performed. The exposure time of these specimens was 40-60 s, followed by washing and drying. For EBSD, the final surface was prepared by electro-polishing in a 65% orthophosphoric acid + 15% sulphuric acid + 6% chromic anhydride + 14% water solution [28]. The electro-polishing parameters were: temperature 70-90 °C, anodic current density, 1 A/cm^2, voltage 23 V and exposure time 19 s.

For microstructural analysis, several methods were used: scanning electron microscopy (SEM) using a Tscan Mira 3 LMU facility, and energy dispersive X-Ray spectroscopy (EDS). EBSD analysis was conducted using a Zeiss SUPRA 55 VP scanning-electron microscope (FEG-SEM) operating at 20 kV. The EBSD data acquisition and analysis was undertaken using EDAX-TSL Orientation Imaging Microscopy with OIM^{TM} software.

To support the microstructure characterization Thermo-Calc software version with TCHEA5 High-Entropy Alloy database was used for thermodynamic calculations, which were performed in order to predict phase formation and partitioning under equilibrium and non-equilibrium solidification conditions, associated solidification path, solidification temperature range, and constituent phases at the end of solidification [29,30]. Solidification calculations were performed for the experimentally-prepared alloy compositions.

Mechanical properties characterization was performed using indentation. Indentation is the most accurate, theoretically and experimentally confirmed standardized method for determining the physical and mechanical properties at the micro and nanometre levels for materials consisting of fine structure and local gradient of material properties [31]. Nanoindentation is a test based on the method of Oliver and Parr [32] to determine the hardness and modulus of elasticity from indentation diagrams that are recorded by continuous penetration of a Berkovich diamond indenter [33]. The ratio of a material's hardness, H, to its Young's modulus, E (H/E), is useful to assess the degree of hardening quickly and efficiently in engineering materials. The H/E ratio characterizes the ability of a material to change shape and size during deformation and can also serve as a qualitative comparative characteristic of the resistance of materials to deformation under mechanical loading and thus reflect its structural state. The Vickers hardness technique was also performed. Tensile testing was utilized on an universal servo-hydraulic complex MTS 318.25 with a maximum force of 250 kN. The samples for testing were cuted from the middle part of the bulk billet along the scanning direction.

3. Results and discussion

The essential part of the additively manufactured HEA billet is structure-properties characterization [34,35]. In the current study, the whole billet is considered from the middle zone, as it reflects a representative volume, and the thermal cycle effect is more homogeneous in this part. But for clarity, the chemical composition measurements were made in all zones, namely the bottom, middle, and top of the billet. EDX spectroscopy, X-Ray maps of the distribution of the principal elements are presented in Fig. 3 a,d. The uniform formation of a single-phase alloy and the uniform distribution of chemical elements are also observed. The liquation of manganese is insignificant, which is conditioned by solidification kinetics, namely the element with a relatively low melting point (1250 °C for Mn) is segregating into the interdendritic regions. The slight segregation of nickel is caused by the nonequilibrium solidification process i.e. relatively higher cooling speed compared to conventional melting processes. Chemical composition analysis made from the bottom middle and top part of the WAAM HEA billet (Table 3) has shown uniform distribution through the height of the sample.

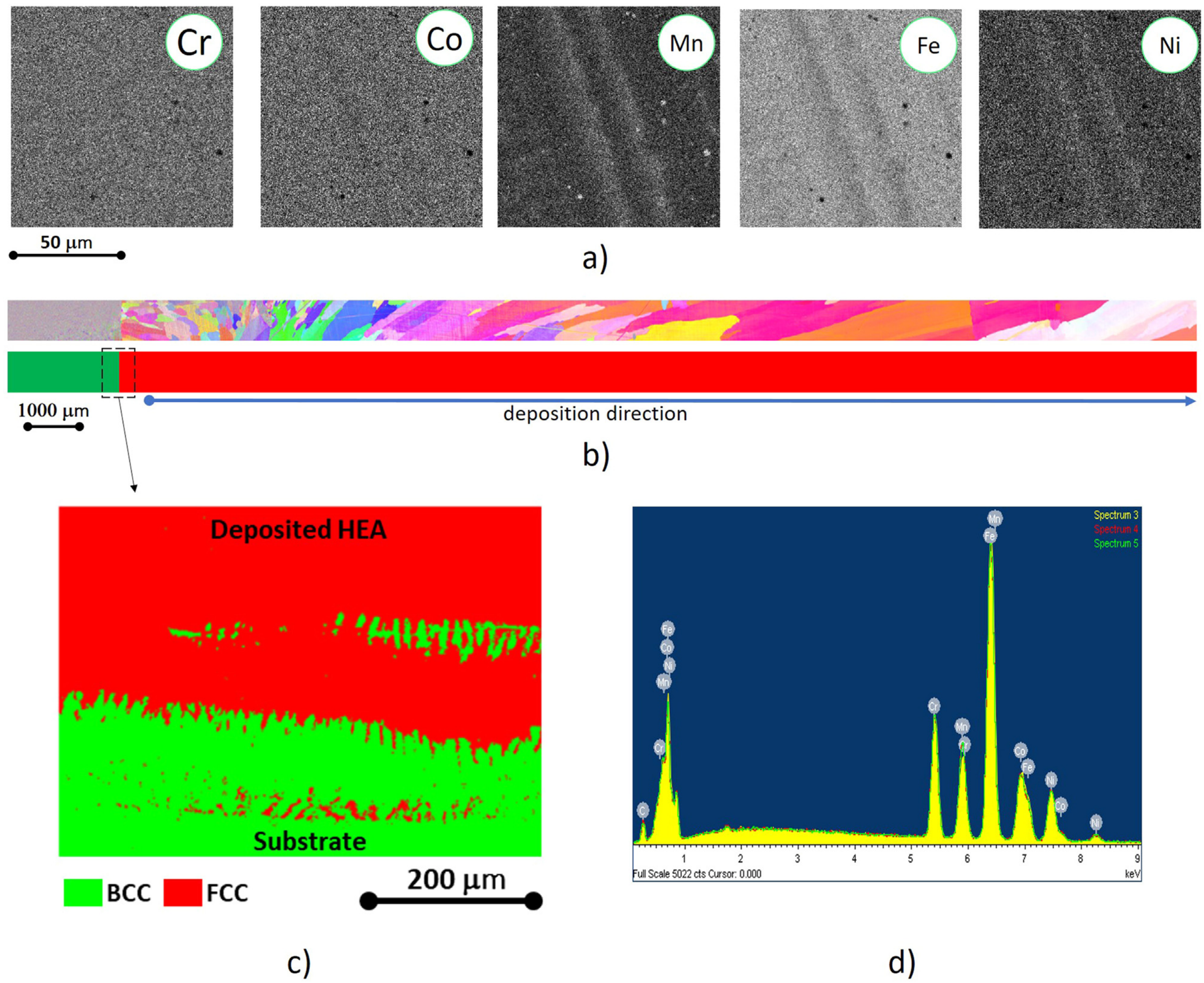

Fig. 3. Microstructure characterization of the WAAMed HEA billet: X-Ray maps for the selected area from the middle part of the billet (a), EBSD IPF and phase maps (b), EBSD phase map for interface substrate-deposition (c), EDX spectra for 1000 mm^2 area of the middle part zone (d).

Table 3
Chemical composition of WAAM HEA billet, at%.

Zone	Cr	Mn	Fe	Co	Ni
Bottom	13.80	11.69	49.38	12.40	12.73
Middle	13.82	11.64	49.33	12.44	12.77
Top	13.85	11.93	49.20	12.17	12.85

There is a slight deviation of the chromium and nikel-allying elements but at the error limit, its values are quite stable. The difference between the volume fraction of Cr compared to Ni and Co could be conditioned by its content in the welding wire due to possible dispersion during filler powder mixture preparation.

A cross-sectional EBSD map of the fabricated WAAM HEA is detailed in (Fig. 3 b). A defect-free component was obtained (in means micro/macro pores voids cracks hot cracks etc.). The microstructure of the WAAM part changed from a mixed of equiaxed and columnar grains near the steel substrate to a fully columnar grain structure, highlighting the typical texture of WAAM-fabricated parts.

The WAAM part is composed of an FCC phase along the entire height with the exception of the first deposited layer. Here, the dilution with the substrate lead to the formation of trace amounts of BCC phase, as shown in (Fig. 3 c). The presence of the substrate metal with BCC lattice in deposited metal and vice versa are commonly known phenomena. This effect is explained by the 'Marangoni effect' [36–38] which describes mixing metal in the welding bath due to the convection flow of the molten metal under the arc pressure.

Considering the chemical composition of the alloy, as obtained by EDX, the predicted solidification path based on the Scheil-Gulliver equation was obtained. The solidification temperature range is calculated as follows: liquidus T = 1410 °C, solidus T = 1390 °C. A fully FCC structure is predicted, which is in good agreement with the EBSD data obtained across the WAAM part, except for the first layer due ro the dilution with the substrate.

Further SEM investigation reveals interesting microstructure peculiarities (Fig. 4). In SE mode (this mode reveals morphological contrast) there are grain- and subgrain-structures which are visible. The grains have a columnar structure characteristic for the deposited metal and are oriented toward the building direction. While in BSE mode (this mode reveals phase contrast) there is no microstructural contrast. This is related to the homogenous composition of the fabricated material, which renders the formation of a single FCC solid solution.

According to the performed mechanical testing (Fig. 5 a), the considered bulk billet of the HEA possesses the following mechanical properties: YS = 275 ± 15 MPa, UTS = 500 ± 10 MPa, with 1.81 plasticity

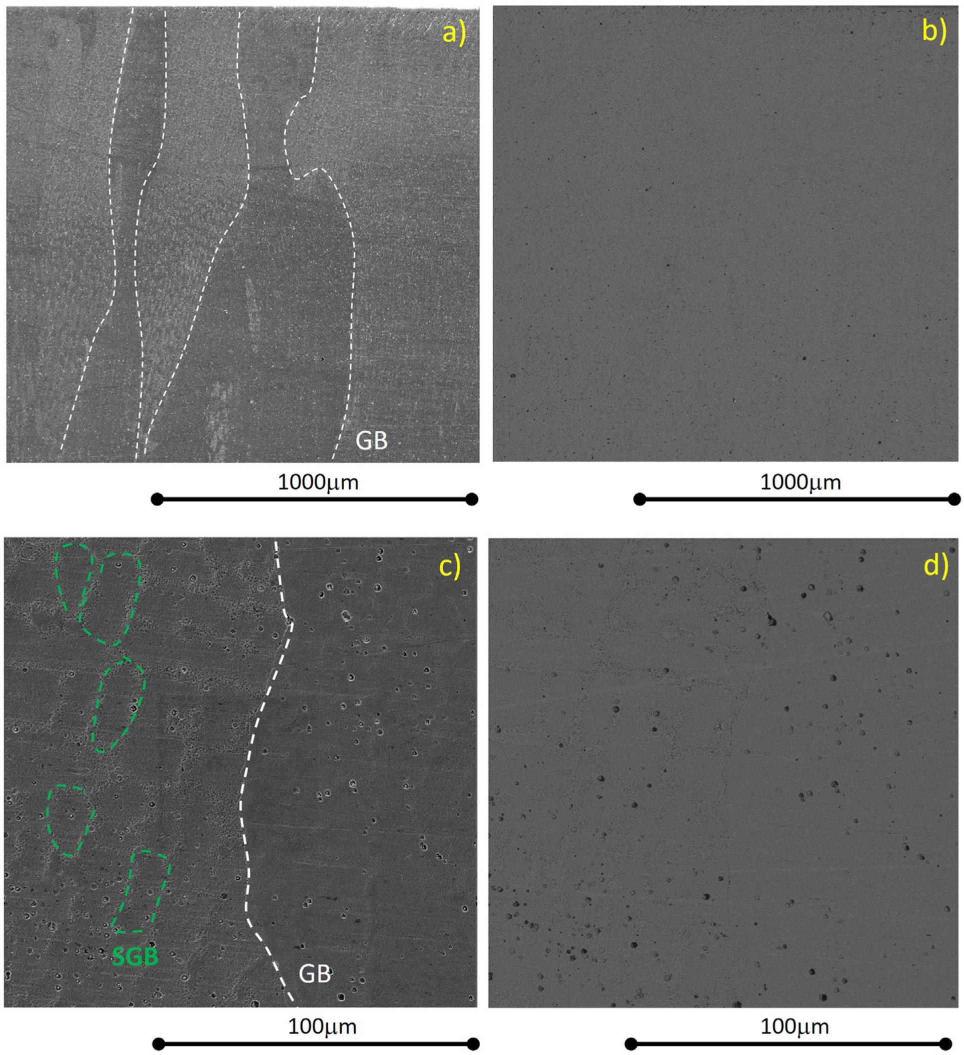

Fig. 4. SEM analysis of the WAAMed HEA bulk sample, middle part: SE-mode (a, c), BSE mode (b,d). GB – grain boundary, SBG – sub-grain baundary.

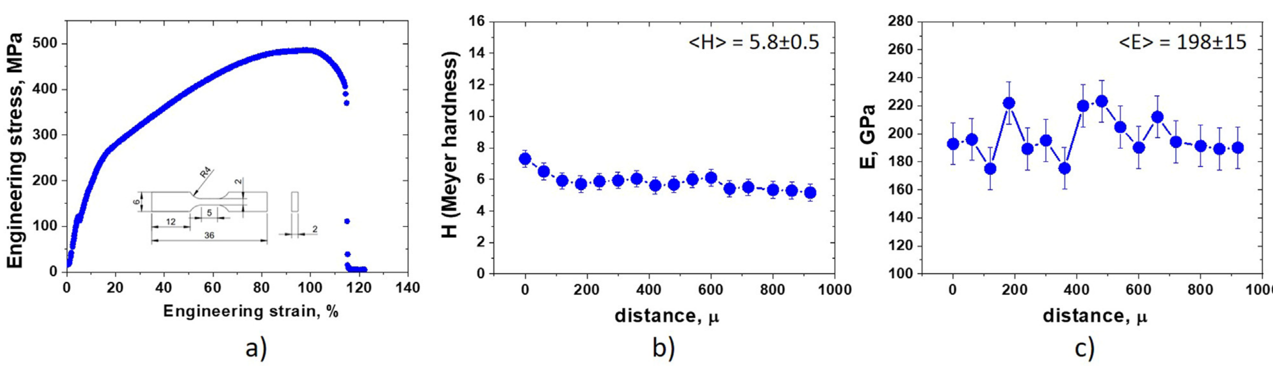

Fig. 5. Mechanical properties of the WAAM HEA: Tensile test (a), Meyer hardness (b), Young's modulus (c).

resource determined as the ratio between UTS and YS. The elongation to failure reveals an extremely high level exceeding 100%, which is well correlated with the value of plasticity resource. The Vickers hardness of the deposited HEA at the middle part of the billet is equal to 160 ± 8 HV. Uniform distribution of the mechanical properties (Meyer hardness) as well as Young's modulus (*E*) within 10% error is observed (Fig. 5 b, c). The low dispersions of the Meyer hardness are evidence of the homogeneity of grain structure across the WAAM part. While higher dispersion of the Young's modulus *E* could be caused by minor chemical fluctuations, which would render slight changes in this property.

3. SWOT analysis of research results

3.1. Strengths

The positive effect of the present research consists of the development methodology for the fabrication of a dedicated HEA wire feedstock to be used for WAAM. The proposed methodology enables the possibility of the fabrication of large structural components based on HEAs and fabricated with WAAM using inexpensive and safer wire feedstock.

3.2. Weaknesses

WAAM of HEAs is still very insipient. Thus, significant research efforts are necessary to unveil potential alloy compositions and to determine the microstructure evolution during arc-based AM processes.

3.3. Opportunities

From the above mentioned, it follows that the prospects for further research consist in establishing the details of the physical and mechanical properties of the WAAM HEA produced with MPCW (changing processing conditions and/or feedstock material condition), which will reduce the adjustment time of the technology when it is incorporated into upscaled production.

3.4. Threats

To obtain an economic effect, it is needed to go through the stage of implementation and testing of the MPCW technology in real production conditions.

4. Conclusions

Metal powder cored wire arc additive manufacturing of HEA was successfully performed. The proposed technical solution can be used for additive manufacturing of HEA using GMAW as the heat source. The filling materials used for the wire feedstock include components in equal molar fraction of cobalt, manganese, chromium, nickel, while the remaining is an Fe shell. Defect-free parts were obtained with a single FCC structure developing along the height of the wall. The mechanical properties were seen to be homogenous along the height of the fabricated material. This work opens the door for the implementation of WAAM for the production of structural components based on HEAs.

Declaration of Competing Interest

The authors declare the following financial interests/personal relationships which may be considered as potential competing interests:

One of the authors of this article is part of the Editorial Board of the journal. To avoid potential conflicts of interest, the responsibility for the editorial and peer-review process of this article lies with the journal's other editors. Furthermore, the authors of this article were removed from the peer review process and had no and will not have any access to confidential information related to the editorial process of this article.

CRediT authorship contribution statement

Anatoliy Zavdoveev: Conceptualization, Methodology, Supervision. **Andrey Klapatyuk:** Conceptualization, Methodology. **Thierry Baudin:** Conceptualization, Methodology. **Eric MacDonald:** Conceptualization, Methodology. **Dhanesh Mohan:** Data curation, Writing – original draft. **J.P. Oliveira:** Data curation, Formal analysis, Validation, Writing – original draft, Writing – review & editing. **Alex Gajvoronskiy:** Supervision. **Valeriy Poznyakov:** Supervision. **Hyoung Seop Kim:** Supervision. **Francois Brisset:** Data curation, Writing – original draft. **Maksym Khokhlov:** Data curation, Writing – original draft. **Mark Heaton:** Data curation, Writing – original draft. **Massimo Rogante:** Data curation, Writing – original draft. **Mykola Skoryk:** Data curation, Writing – original draft. **Dmitry Vedel:** Data curation, Writing – original draft. **Roman Kozin:** Data curation, Writing – original draft. **Illya Klochkov:** Data curation, Writing – original draft. **Sviatoslav Motrunich:** Data curation, Writing – original draft.

Data Availability

Data will be made available on request.

Acknowledgments

This work was supported by the National Academy of Sciences of Ukraine [Grant Number 0117U001666] and National Research Foundation of Korea (NRF) grant funded by the Korea government (MSIP) (NRF-2021R1A2C3006662). JPO acknowledges funding by national funds from FCT - Fundação para a Ciência e a Tecnologia, I.P., in the scope of the projects LA/P/0037/2020, UIDP/50025/2020 and UIDB/50025/2020 of the Associate Laboratory Institute of Nanostructures, Nanomodelling and Nanofabrication – i3N. We would like to thank the Murchison Endowment at the University of Texas at El Paso.The authors are grateful to Dr. M. Speicher (Wissenschaftlerin bei Universität Stuttgart), Dr. S. Moskalyuk (G. V. Kurdyumov Institute of Metal Physics of the NAS of Ukraine), Eng. E.Los and T.Solomijchuk (Paton Electric Welding Institute of NAS of Ukraine) for help in experiments.

Reference

[1] K. Wu, N. Ding, T. Yin, M. Zeng, Z. Liang, Effects of single and double pulses on microstructure and mechanical properties of weld joints during high-power double-wire GMAW, J. Manuf. Process. 35 (2018) 728–734, doi:10.1016/j.jmapro.2018.08.025.

[2] G. Bernd, H. Anton, C. Dhiraj, E.H. Chang, P.E. George, R.O. Ritchie, A fracture-resistant high-entropy alloy for cryogenic applications, Science (80-.) 345 (2014) 1153–1158, doi:10.1126/science.1254581.

[3] A. Takeuchi, K. Amiya, T. Wada, K. Yubuta, W. Zhang, High-entropy alloys with a hexagonal close-packed structure designed by equi-atomic alloy strategy and binary phase diagrams, JOM 66 (2014) 1984–1992, doi:10.1007/s11837-014-1085-x.

[4] C.L. Tracy, S. Park, D.R. Rittman, S.J. Zinkle, H. Bei, M. Lang, R.C. Ewing, W.L. Mao, High pressure synthesis of a hexagonal close-packed phase of the high-entropy alloy CrMnFeCoNi, Nat. Commun. 8 (2017) 15634, doi:10.1038/ncomms15634.

[5] Y.J. Liang, L. Wang, Y. Wen, B. Cheng, Q. Wu, T. Cao, Q. Xiao, Y. Xue, G. Sha, Y. Wang, Y. Ren, X. Li, L. Wang, F. Wang, H. Cai, High-content ductile coherent nanoprecipitates achieve ultrastrong high-entropy alloys, Nat. Commun. 9 (2018) 4063, doi:10.1038/s41467-018-06600-8.

[6] W. Ji, W. Wang, H. Wang, J. Zhang, Y. Wang, F. Zhang, Z. Fu, Short communication, Intermetallics 56 (2015) 24–27, doi:10.1016/j.intermet.2014.08.008.

[7] Z. Tang, T. Yuan, C.W. Tsai, J.W. Yeh, C.D. Lundin, P.K. Liaw, Fatigue behavior of a wrought $Al_{0.5}$CoCrCuFeNi two-phase high-entropy alloy, Acta Mater. 99 (2015) 247–258, doi:10.1016/j.actamat.2015.07.004.

[8] P. Wang, P. Huang, F.L. Ng, W.J. Sin, S. Lu, M.L.S. Nai, Z. Dong, J. Wei, Additively manufactured CoCrFeNiMn high-entropy alloy via pre-alloyed powder, Mater. Des. 168 (2019) 107576, doi:10.1016/j.matdes.2018.107576.

[9] R. Li, P. Niu, T. Yuan, P. Cao, C. Chen, K. Zhou, Selective laser melting of an equiatomic CoCrFeMnNi high-entropy alloy: processability, non-equilibrium microstructure and mechanical property, J. Alloys Compd. 746 (2018) 125–134, doi:10.1016/j.jallcom.2018.02.298.

[10] A. Ostovari Moghaddam, N.A. Shaburova, M.N. Samodurova, A. Abdollahzadeh, E.A. Trofimov, Additive manufacturing of high entropy alloys: a practical review, J. Mater. Sci. Technol. 77 (2021) 131–162, doi:10.1016/j.jmst.2020.11.029.

[11] T. Fujieda, H. Shiratori, K. Kuwabara, T. Kato, K. Yamanaka, Y. Koizumi, A. Chiba, First demonstration of promising selective electron beam melting method for utilizing high-entropy alloys as engineering materials, Mater. Lett. 159 (2015) 12–15, doi:10.1016/j.matlet.2015.06.046.

[12] K. Kuwabara, H. Shiratori, T. Fujieda, K. Yamanaka, Y. Koizumi, A. Chiba, Mechanical and corrosion properties of AlCoCrFeNi high-entropy alloy fabricated with selective electron beam melting, Addit. Manuf. 23 (2018) 264–271, doi:10.1016/j.addma.2018.06.006.

[13] X.H. An, X. Liao, Z.G. Zhu, B. Nguyen, F. Ng, P.K. Liaw, M.L.S. Nai, J. Wei, Hierarchical microstructure and strengthening mechanisms of a CoCrFeNiMn high entropy alloy additively manufactured by selective laser melting, Scr. Mater. 154 (2018), doi:10.1016/j.scriptamat.2018.05.015.

[14] A. Piglione, B. Dovgyy, C. Liu, C.M. Gourlay, P.A. Hooper, M.S. Pham, Printability and microstructure of the CoCrFeMnNi high-entropy alloy fabricated by laser powder bed fusion, Mater. Lett. 224 (2018) 22–25, doi:10.1016/j.matlet.2018.04.052.

[15] W. Wu, R. Zhou, B. Wei, S. Ni, Y. Liu, M. Song, Nanosized precipitates and dislocation networks reinforced C-containing CoCrFeNi high-entropy alloy fabricated by selective laser melting, Mater. Charact. (2018) 605–610, doi:10.1016/jmatchar201808019.

[16] T. Borkar, V. Chaudhary, B. Gwalani, D. Choudhuri, C.V Mikler, V. Soni, T. Alam, R.V. Ramanujan, R. Banerjee, A combinatorial approach for assessing the magnetic properties of high entropy alloys: role of Cr in AlCoxCr1–xFeNi, Adv. Eng. Mater. 19 (2017) 1700048, doi:10.1002/adem.201700048.

[17] Y. Brif, M. Thomas, I. Todd, The use of high-entropy alloys in additive manufacturing, Scr. Mater. 99 (2015), doi:10.1016/j.scriptamat.2014.11.037.

[18] R. Zhou, Y. Liu, B. Liu, L. Jia, Q. Fang, Precipitation behavior of selective laser melted $FeCoCrNiC_{0.05}$ high entropy alloy, Intermetallics 106 (2019) 20–25, doi:10.1016/j.intermet.2018.12.001.

[19] T. Fujieda, H. Shiratori, K. Kuwabara, M. Hirota, T. Kato, K. Yamanaka, Y. Koizumi, A. Chiba, S. Watanabe, CoCrFeNiTi-based high-entropy alloy with superior tensile strength and corrosion resistance achieved by a combination of additive manufacturing using selective electron beam melting and solution treatment, Mater. Lett. 189 (2017) 148–151, doi:10.1016/j.matlet.2016.11.026.
[20] H. Shiratori, T. Fujieda, K. Yamanaka, Y. Koizumi, K. Kuwabara, T. Kato, A. Chiba, Relationship between the microstructure and mechanical properties of an equiatomic AlCoCrFeNi high-entropy alloy fabricated by selective electron beam melting, Mater. Sci. Eng. A. 656 (2016) 39–46, doi:10.1016/j.msea.2016.01.019.
[21] F. Zhang, S. Zhao, K. Jin, H. Bei, D. Popov, Pressure-induced fcc to hcp phase transition in Ni-based high entropy solid solution alloys, Appl. Phys. Lett. 110 (2017) v., doi:10.1063/14973627.
[22] P.D. Niu, R.D. Li, T.C. Yuan, S.Y. Zhu, C. Chen, M.B. Wang, L. Huang, Microstructures and properties of an equimolar AlCoCrFeNi high entropy alloy printed by selective laser melting, Intermetallics 104 (2019) 24–32, doi:10.1016/j.intermet.2018.10.018.
[23] S. Luo, C. Zhao, Y. Su, Q. Liu, Z. Wang, Selective laser melting of dual phase AlCrCuFeNix high entropy alloys: formability, heterogeneous microstructures and deformation mechanisms, Addit. Manuf. 31 (2020) 100925, doi:10.1016/j.addma.2019.100925.
[24] D. Lin, L. Xu, H. Jing, Y. Han, L. Zhao, F. Minami, Effects of annealing on the structure and mechanical properties of FeCoCrNi high-entropy alloy fabricated via selective laser melting, Addit. Manuf. 32 (2020) 101058, doi:10.1016/j.addma.2020.101058.
[25] M.R.U. Ahsan, G.J. Seo, X. Fan, P.K. Liaw, S. Motaman, C. Haase, D.B. Kim, Effects of process parameters on bead shape, microstructure, and mechanical properties in wire + arc additive manufacturing of $Al_{0.1}$CoCrFeNi high-entropy alloy, J. Manuf. Process. 68 (2021) 1314–1327, doi:10.1016/j.jmapro.2021.06.047.
[26] Q. Shen, X. Kong, X. Chen, Fabrication of bulk Al-Co-Cr-Fe-Ni high-entropy alloy using combined cable wire arc additive manufacturing (CCW-AAM): microstructure and mechanical properties, J. Mater. Sci. Technol. 74 (2021) 136–142, doi:10.1016/j.jmst.2020.10.037.
[27] A. Zavdoveev, T. Baudin, E. Pashinska, H.S. Kim, F. Brisset, M. Heaton, V. Poznyakov, M. Rogante, V. Tkachenko, I. Klochkov, M. Skoryk, Continuous severe plastic deformation of low-carbon steel: physical–mechanical properties and multiscale structure analysis, Steel Res. Int. 92 (2021) 2000482, doi:10.1002/srin.202000482.
[28] A. Zavdoveev, T. Baudin, E. Pashinska, M. Skoryk, Preparation of metallographic specimens for electron backscatter diffraction, Emerg. Mater. Res. 6 (2017) 260–264, doi:10.1680/jemmr.16.00117.
[29] A. Abu-Odeh, E. Galvan, T. Kirk, H. Mao, Q. Chen, P. Mason, R. Malak, R. Arroyave, Exploration of the high entropy alloy space as a constraint satisfaction problem, ArXiv Prepr. ArXiv1712.02442. (2017).
[30] A.C. Martin, J.P. Oliveira, C. Fink, Elemental effects on weld cracking susceptibility in AlxCoCrCuyFeNi high-entropy alloy, Metall. Mater. Trans. A. 51 (2020) 778–787, doi:10.1007/s11661-019-05564-8.
[31] J. Khokhlova, M. Khokhlov, A. Tunik, A. Ishchenko, Nanoindentation of micro weld formed through thin nanolayered filler, in: Nanomechanical Analysis of High Performance Materials, Springer, 2014, pp. 251–262.
[32] W.C. Oliver, G.M. Pharr, An improved technique for determining hardness and elastic modulus using load and displacement sensing indentation experiments, J. Mater. Res. 7 (1992) 1564–1583.
[33] Nano indenters from micro star technologies. Revision 2.3. P.9. (http://www.microstartech.com/index/NANOINDENTERS.pdf).
[34] Y. Guo, H. Su, H. Zhou, Z. Shen, Y. Liu, J. Zhang, L. Liu, H. Fu, Unique strength-ductility balance of $AlCoCrFeNi_{2.1}$ eutectic high entropy alloy with ultra-fine duplex microstructure prepared by selective laser melting, J. Mater. Sci. Technol. 111 (2022) 298–306, doi:10.1016/j.jmst.2021.10.013.
[35] H.S. Yinuo Guo Peixin Yang, Y. Zhao, Z. Shen, Y. Liu, D. Zhao, H. Jiang, J. Zhang, L. Liu, H. Fu, A review of emerging metallic system for high-energy beam additive manufacturing: Al-Co-Cr-Fe-Ni high entropy alloys, Acta Metall. Sin. (Engl. Lett.) 35, 1407-1423 (2022). doi:10.1007/s40195-022-01400-y.
[36] I. Krivtsun, U. Reisgen, O. Semenov, A. Zabirov, Modeling of weld pool phenomena in tungsten inert gas, CO_2-laser and hybrid (TIG+ CO_2-laser) welding, J. Laser Appl. 28 (2016) 22406.
[37] A.M. Torbati, R.M. Miranda, L. Quintino, S. Williams, D. Yapp, Optimization procedures for GMAW of bimetal pipes, J. Mater. Process. Technol. 211 (2011) 1112–1116.
[38] J. Hu, H. Guo, H.L. Tsai, Weld pool dynamics and the formation of ripples in 3D gas metal arc welding, Int. J. Heat Mass Transf. 51 (2008) 2537–2552.